plasticheal

March, 2022

D4.1 STANDARD OPERATING PROCEDURE (SOP) FOR THE APPLICATION OF ANALYTICAL METHODS TO THE DETECTION AND MEASUREMENT OF MNPLS IN BIOLOGICAL TISSUES

Tom Venus, Thomas Loret, Ricardo Marcos Dauder, Alba Hernández Bonilla, Cyrill Bussy, Irina Estrela-Lopis

Document identifier **XXXX**

Version **1**

Dissemination status **Public**

plasticheal

D4.1 STANDARD OPERATING PROCEDURE (SOP) FOR THE APPLICATION OF ANALYTICAL METHODS TO THE DETECTION AND MEASUREMENT OF MNPLS IN BIOLOGICAL TISSUES

Grant Agreement n°:	965196
Project acronym:	PLASTICHEAL
Project title:	Innovative tools to study the impact and mode of action of micro and nanoplastics on human health: towards a knowledge base for risk assessment
Topic:	SC1-BHC-36-2020: Micro- and nano-plastics in our environment: Understanding exposures and impacts on human health
Project Duration:	2021/04/01 – 2025/03/31
Coordinator:	Universitat Autònoma de Barcelona (UAB)
Associated Beneficiaries:	Tyoterveyslaitos Wageningen University & Research (WUR) Danmarks Tekniske Universitet (DTU) Commissariat à l'énergie atomique et aux énergies alternatives (CEA) Fundacion para la Formacion e Investigacion Sanitarias de la Region de Murcia (FFIS) The University of Manchester AIMPLAS - Asociacion de Investigacion de Materiales Plasticos y Conexas Institut National de la Sante et de la Recherche Medicale (Inserm) Helmholtz-zentrum fur Umweltforschung GMBH (UFZ) Universitaet Leipzig

This project has received funding from the European Union's Horizon 2020 research and innovation programme under grant agreement No. 965196

plasticheal

PROJECT No. 965196

Innovative tools to study the impact and mode of action of micro and nanoplastics on human health: towards a knowledge base for risk assessment

HISTORY CHART

Issue	Date	Changed page(s)	Cause of change	Implemented by
0.10		-	Draft	
1.0		ALL	Version 1.0	
2.0		ALL	Version 2.0	

VALIDATION CHART

No.	Action	Beneficiary	Date
1	Prepared		
2	Approved		
3	Released		

This project has received funding from the European Union's Horizon 2020 research and innovation programme under grant agreement No. 965196

plasticheal

TABLE OF CONTENTS

A SOP has been developed and adapted for detection, chemical identification and visualization of MNPLs in biological matrices by means of confocal Raman microscopy (CRM). CRM analyses were performed with an Alpha300 R microscope (WITec GmbH, Germany) equipped with a piezo-scanner (P-500, Physik Instrumente, Karlsruhe, Germany), multi-mode fibers (25 µm, 50 µm and 100 µm in diameter) and a charge-coupled device (CCD) cooled down to -61°C. CRM tool allows for the label-free imaging of MNLPs in complex matrices, such as tissues and cells. Detection of plastic particles in biomatrices can be achieved by discrimination of a plastic specific fingerprint from molecular signatures of different cells, cell components and biomolecules like lipids, proteins, cytochromes, collagen or RNA/DNA [1].

For evaluation purpose, lung tissue slices and broncho-alveolar lavage fluid (BAL) from mice exposed for 24 hours to 50 µg and 150 µg polystyrene (PS) particles (PolyScience Europe GmbH) with a size of 50 nm by a single oropharyngeal aspiration as well as whole drosophila larvae exposed to 800 µg/ml PS particles in medium have been studied. Samples of mice and drosophila have been provided by UNIMAN and UAB, respectively.

This project has received funding from the European Union's Horizon 2020 research and innovation programme under grant agreement No. 965196

plasticheal

1. Control measurements of PS particles and their spectroscopic assignment

As a first measure of detection, the specific spectral signature of the particle in question was determined to reliably detect the particles in cells, tissues and other biological specimens. To achieve this, 50 µl of a 200 µg/µl PS solution with a particle diameter of 50 nm have been drop-casted and then dried on a glass slide. The measurement with the 532 nm laser was done under dry conditions at three different positions on the sample. The laser power and integration time were adjusted to avoid burning of the particles and were set to 37 mW and 5 seconds, respectively. At each position the measurement was repeated 5 times and the obtained spectra were merged subsequently. The Raman spectrum shows a strong band at 1001 cm^{-1}, which is linked to the breathing mode of the aromatic carbon ring (Figure 1). Other bands correspond to the ring deformation mode (621 cm^{-1}), CH out of plane and in plane deformation (795/1031 cm^{-1}), C–C stretching (1155 cm^{-1}), CH_2 scissoring (1450 cm^{-1}), ring skeletal stretch (1602 cm^{-1}), symmetric (2852 cm^{-1}) and antisymmetric (2904 cm^{-1}) CH_2 aliphatic stretching modes as well as overlapping bands at 3054 cm^{-1} due to the C–H bonds stretching on the benzene ring [2, 3] .

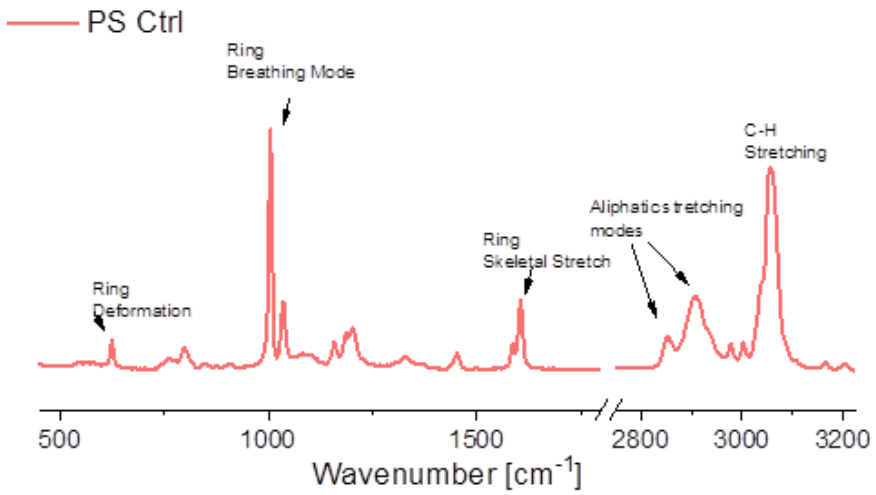

Figure 1: Raman spectrum of PS particles dried on glass substrate. The spectrum was recorded using 532 nm laser at power of 37 mW.

This project has received funding from the European Union's Horizon 2020 research and innovation programme under grant agreement No. 965196

plasticheal

2. Control measurements of biological samples

The measurement of biological samples requires several parameters adjusted to yield reasonable and reliable results. Depending on the choice of the laser and its power, the substrate, measuring conditions and the objective of the measurement several adjustments must be done in order to prevent the disintegration of the sample through burning or impairment of the outcome by fluorescence.

2.1. Laser selection

Two lasers have been tested regarding their ability to burn the sample, produce unwanted fluorescence or luminescence and to provide spectral information about the sample. The 532nm laser has been shown to be very effective. The resulting spectra contains a large yield of biological relevant Raman bands (stretching & deformation CH_2/CH_3 and amide modes), which can be explained by Raman scattering intensity being inversely proportional to the fourth power of the incident light wavelength, i.e. shorter wavelengths produce more Raman photons. However, this has the downside of potentially burning the sample around the laser spot, which is indicated by the G and D bands of charred organic matter that are apparent in the spectra (Figure). The 532 nm laser can also cause a fluorescence background in biological samples containing tryptophan and tyrosine side chains of proteins. Lung tissue sections of mice produce very little autofluorescence. In contrast, very strong fluorescence background was observed by the measurement of Drosophila larvae (Figure 2). The 785 nm laser is gentler to the sample and causes low fluorescence background, but also yield less signal intensity. The utilization of 785 nm laser has an additional drawback, because it produces a broad photo luminescence peak originated from glass slide used as a tissue substrate [4]. Figure 2 shows a summary of unfavorable effects that impair the detection of biomolecules and particles. The effects depend on the choice of the laser, the substrate and the measuring conditions and need to be avoided.

This project has received funding from the European Union's Horizon 2020 research and innovation programme under grant agreement No. 965196

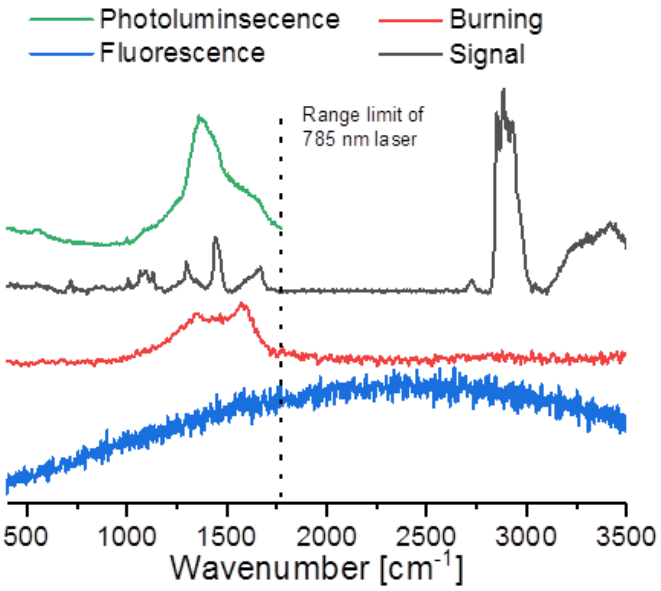

Figure 2: Influence of photoluminescence, fluorescence and sample burning on signal detection. All three effects impair the proper detection of biomolecules and particles. Raman spectrum from alveolar septum was recorded at optimized conditions (black line) and reveals typical fingerprint of lipid bodies located in ATII cell. The dotted line shows the high frequency range limit of the 785 nm laser.

2.2. Adjustment of laser power and integration time

The less power is used, the longer integration time is needed to achieve the reasonable signal intensity and to avoid sample burning. Both parameters have been adjusted for lung tissue slices (a) in dry state and (b) immersed in PBS solution.

Dry tissue samples

The power of the 532 nm laser had to be reduced from 37 to 5 mW in dry tissue slices. Application of laser power of 10 mW and 15 mW caused the samples to burn and disintegrate. Figure 3 shows the measurement of lung tissue slices from mice. The two squares, red and blue, indicate the areas that were measured with CRM by applying laser power of 15 mW and 10 mW, respectively. In both cases, the samples started to burn, which makes it impossible to get a clear image of the structure of the alveolar septum. The Raman spectrum reveals two typical burning G and D bands by using 10 mW (red line). The utilization of 5 mW power of laser allows to get tissue relevant spectrum containing information about lipids, proteins and other biomolecules (e.g. CH_2, CH_3, amid, amino acid and C=C bands). Since the power has to be reduced, the signal-to-noise ratio of the spectra is very low. To compensate for this the integration time of the measurement must be increased to 0.3 s to compensate for the low laser power. However, this also increases the overall measuring time of images. As the 785 nm laser does not cause burning effects, a maximum laser power may be applied for tissue mapping measurements.

This project has received funding from the European Union's Horizon 2020 research and innovation programme under grant agreement No. 965196

plasticheal

Nonetheless, an integration time of 0.3 s to 0.5 s must be used to get signal/noise ratio similar to that at utilization of 532 nm laser.

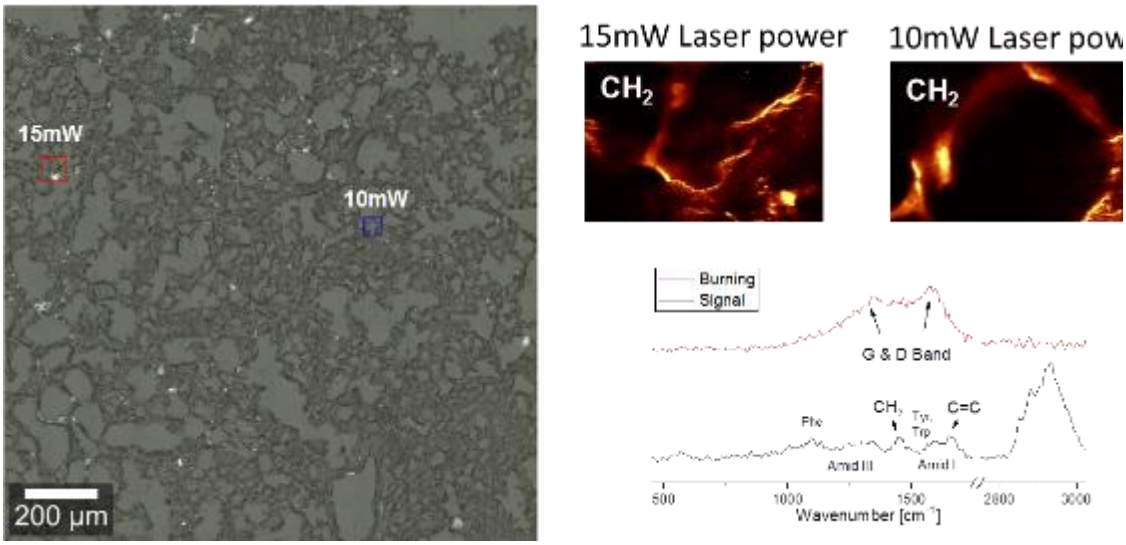

Figure 3: The measurement of the cryo-sections of mouse lung tissue by using 532 nm laser in dry conditions. The squares on bright field image indicate measured areas (left). CRM images show CH2 distribution in lung septum using 15 mW and 10 mW laser power in red and blue squares, respectively. In both cases no clear visualization of the alveolar septum possible (right Top). Raman spectra of burned and unburned tissue in alveolar septum (right bottom).

Wet tissue samples

To circumvent these drawbacks the tissue can be placed in PBS buffer and the measurement can be done under wet conditions using a specialized wet objective with a magnification of 63 and an aperture of 1.0. This allowed the usage of the 532 nm laser with a maximum power of 37 mW with 0.07 s to 0.1s integration time, which thus reduces measurement time of image drastically. A negative aspect of measuring samples in wet conditions is the risk that the sample might swim off. The use of fibronectin coated substrate or adhesion slides Superfrost® may solve this problem.

2.3. Sample substrates

In order to reduce unwanted signals, the choice of tissue substrate of the sample is also important. Glass, quartz and $CaFl_2$ substrate are all Raman active and thus have specific bands that can interfere with ones originated from the biosamples (e.g. BAL cells, culture cells). Using tissue slices of 10 to 20 µm thick allows overcome this problem by adjusting of the laser confocal plane far enough from substrate, where its signal is negligible.

This project has received funding from the European Union's Horizon 2020 research and innovation programme under grant agreement No. 965196

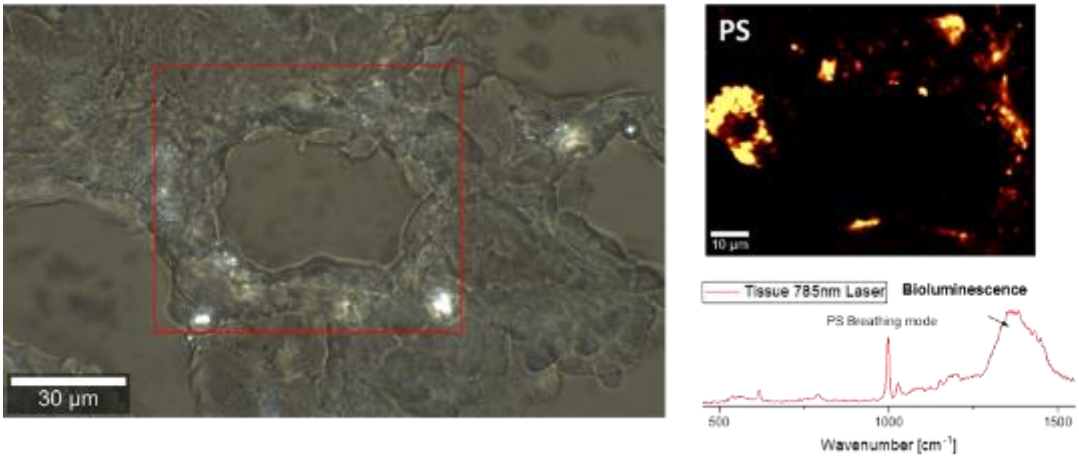

Figure 4: Visualization of lung tissue of mice exposed to 150 µg PS for 24 hours by using 785 nm laser. Bright-field image with the red square, where CRM image was recorded (left); CRM image shows a distribution of PS signal over the measured area (top right). Raman spectrum of tissue reveals notable photoluminescence peak and PS signal at 1001 cm^{-1} (bottom right).

The glass slide as a tissue substrate cannot be applied when using the 785 nm laser, since the excitation wavelength produces a strong photoluminescence signal, which was persistently present in the obtained spectra, regardless of the position of confocal plane from glass substrate (Error! Reference source not found.4 bottom right). The photoluminescence strongly covers signals from biomolecules and makes it impossible to visualize the tissue. However, visualization of PS particles within mouse lung tissue was still possible by analysis of integral intensity of the breathing mode of the aromatic carbon ring of PS at 1001 cm^{-1} (Figure 4 top right). Quartz slides, silicium wafer or $CaFl_2$ substrates are recommended for CRM measurement of tissue sections if a 785 nm laser is applied.

Table 1 summarizes the optimized set up parameters used in figure 4, which can be used as a first approach for detection of plastic particles in biomatrices.

3. Samples of animals exposed to particles

The CRM method has been tested and adapted for detection of plastic particles in three biological specimens, such as lung tissue slices and cells of bronchoalveolar lavage from mice exposed to PS particles, or drosophila larvae also exposed to PS particles.

3.1. Tissue slices

The analyzed samples were lung tissue sections from mice that were exposed to a bolus of 50 µg or 150 µg of PS particles for 24 hours. The sections of 10 µm or 20 µm thick were cut from formalin fixed paraffin embedded tissue. Furthermore, cryosections fixed with methanol or paraformaldehyde have been analyzed as well. CRM images were conducted by using the 532 nm laser under wet conditions with a water-immersed objective x63/1.0, a 50 µm pinhole, 0.1 s integration time and a detector grating of 600g/mm.

This project has received funding from the European Union's Horizon 2020 research and innovation programme under grant agreement No. 965196

plasticheal

3.1.1. Tissue preparation methods

The embedding of tissues in a paraffin block and subsequent cutting into slices is a standard procedure for histology. For CRM measurement, the paraffin has to be removed out of the tissue sections since the paraffin signal strongly interferes with signals from the tissue. However, removing the paraffin with xylol treatment (at least 3 times for 10 minutes) also depletes the lipid bodies out of the tissue samples. Other cellular compartments, such a nuclei, mitochondria or collagen are not affected by xylol treatment so strongly. The paraffin embedding maintains the structural integrity of the sample, which allows the better spatial location of PS particles in the sample (Figure 2). Figure 5 shows measurement of lung tissue section of mice exposed to 150 µg PS for 24 hours. Although the sample was treated 6 times for 10 minutes with xylol, a fraction of paraffin remains in the sample. However, it was still possible to visualize protein and the PS particle distributions in the sample.

Cryo-sections fixed with PFA do not need any further treatment. PFA fixation has the distinct advantage to preserve lipids inside the tissue. Visualization of lipid distribution allows distinguishing different cell types in the septum, such as ATII and ATI cells. Furthermore, spectroscopic information from lipids in tissue could also act as a biomarker for adverse effects. There might be a loss of structural integrity, since the frozen tissue is not embedded in an external matrix, like paraffin. However, the spectral information of biomolecules is rich and interference-free.

This project has received funding from the European Union's Horizon 2020 research and innovation programme under grant agreement No. 965196

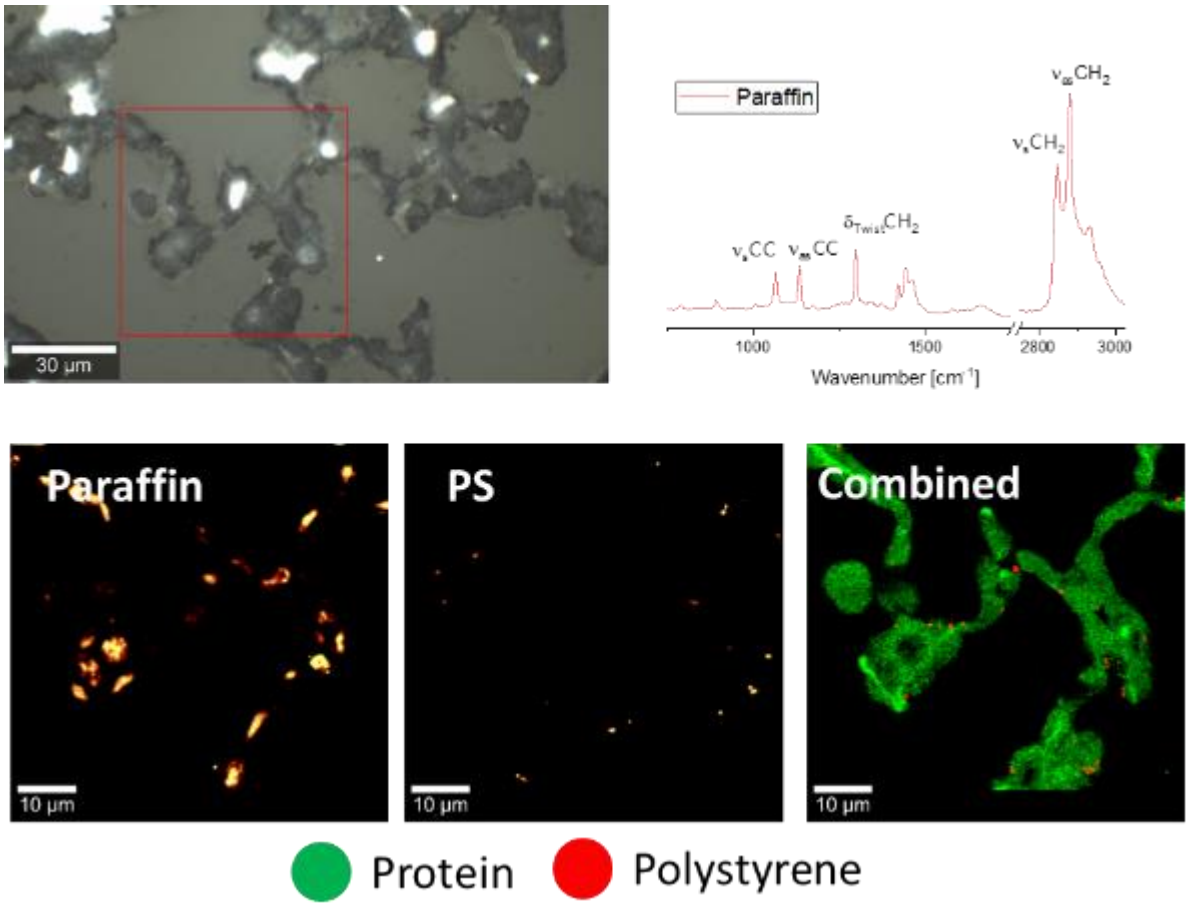

Figure 2: CRM measurement of xylol treated paraffin embedded lung tissue of mice exposed to 150µg PS for 24 hours using 532 nm laser. Bright-field image of alveolar septum (**top left**). CRM spectrum extracted from paraffin accumulation in the septum (**top right**). Distribution of paraffin and PS in the alveolar septum. The color-coded image indicates the uptake of PS particles into the septum (**bottom**).

Methanol fixation of cryo-sections has the drawbacks of both sample preparation methods, PFA fixed frozen and paraffin embedded tissues. On the one hand methanol treatment decomposes lipids in the cells and on the other hand cryo-section offers no protection of the structural integrity of the sample.

PS particles were detectable with all three tissue preparation methods. However, PFA fixed cryo-section of tissue may be recommended as the best one.

3.1.2. Spectroscopic Histology

The usage of well-established Raman fingerprints for different biomolecules, cellular compartments and tissue cell types allowed the visualization of the alveolar septum, erythrocytes, nuclei, lipids and proteins. The use of highly specific bands found in the respective Raman spectra of plastic particles enables the label-free identification of the chemical composition of plastics within tissues, and thus the discrimination between biomolecules and particles. Especially the fingerprint region between 800 cm^{-1} and 1800 cm^{-1} is

This project has received funding from the European Union's Horizon 2020 research and innovation programme under grant agreement No. 965196

suitable for the identification of specific biomolecule bonds [1, 5]. In biological samples, numerous prominent bands in this region are lipid, protein as well as DNA related. The bands at 1263 cm^{-1} (=C-H), 1444 cm^{-1} (CH_2), 1658 cm^{-1} (C=C) and 1740 cm^{-1} (C=O) are assigned to deformation and stretching modes in the lipid spectrum of lipid bodies (LBs) [6]. The Raman band at 1086 cm^{-1} is associated to the stretching mode of PO_2^- groups in phospholipids widespread in membranes and lipid bodies. Bands at 785 cm^{-1}, 1093 cm^{-1}, 1340 cm^{-1}; 785 cm^{-1} correspond to ring breathing modes of the pyrimidine bases and the vibration of the DNA backbone (O-P-O), 1093 cm^{-1} relates to the symmetric PO_2^- stretching vibration of the DNA and the peak at 1340 cm^{-1} is associated with *in plane* vibration of adenine and guanine rings (Figure 3). Figure 6 shows the spectra of several biomolecules, cellular and tissue compartments obtained from analyzed tissue sections.

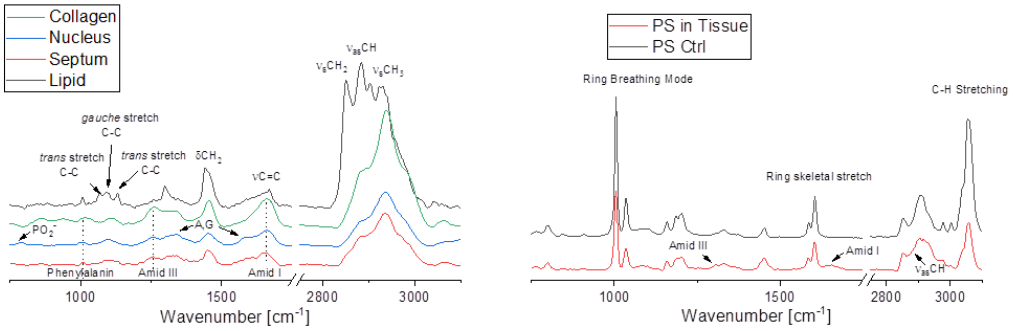

Figure 3: Raman spectra of cryo-sections from lung tissue of mice: Raman spectra of collagen, nuclei, lipids and the septum (**left**). Detection of PS particles on glass substrate and in tissue slice of mouse exposed to 150 µg PS (**right**).

This project has received funding from the European Union's Horizon 2020 research and innovation programme under grant agreement No. 965196

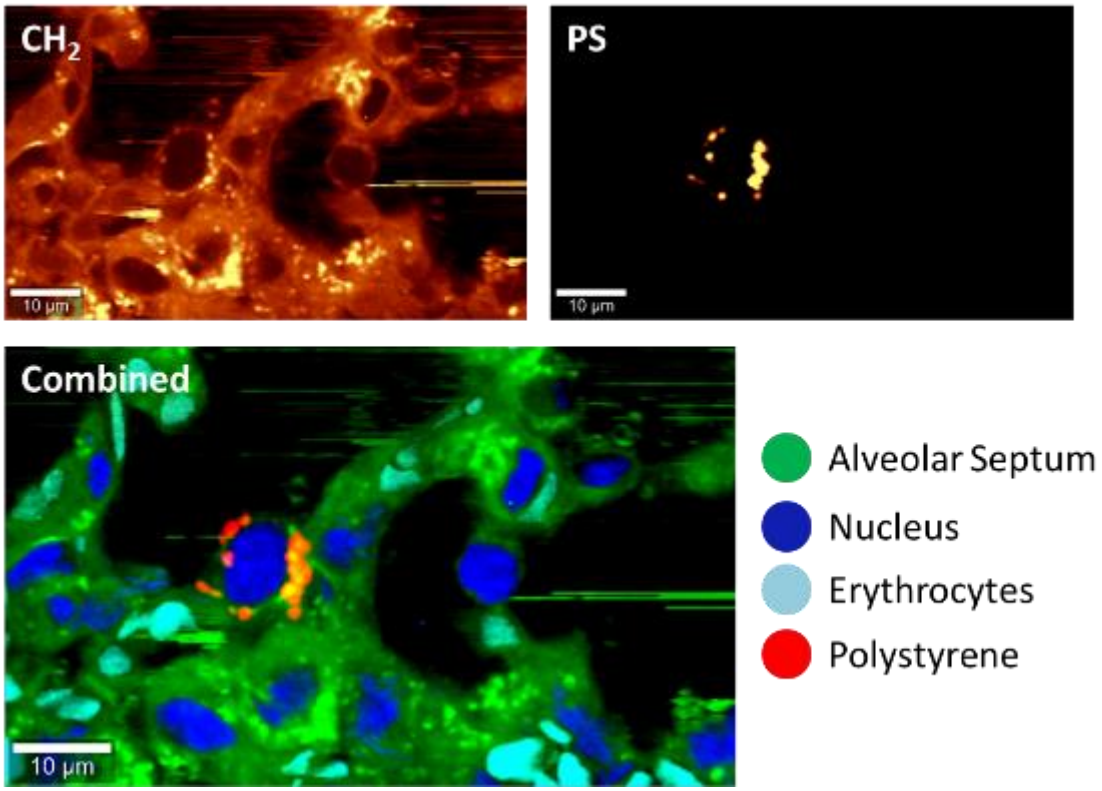

Figure 4: CRM images of lung tissue of mice exposed to 150µg for 24 hours. The distribution of integral intensity of stretching CH_2 band indicates the location of lipid bodies inside the septum (**top left**). Distribution of PS particles in the sample (**top right**). The color-coded image represents the overlapping of proteins, nucleus, erythrocytes and PS particles in the cells of the septum (**bottom**).

The utilization of specific Raman bands allows the detailed visualization of the tissue and a clear determination of particle uptake in certain regions. In Figure 6 (right) Raman spectrum reveals lipid and protein related bands, which have been simultaneously detected with that from PS particles. PS particles were detected and visualized in lung tissue sections of mice exposed to 150 µg as well as 50 µg particles (Figure 47 & Figure 58). The tissue sections were prepared by PFA fixation of cryo-sections. Figure 7 shows the distributions of lipids, proteins, PS particles as well as localization of nucleus and erythrocytes in alveolar septum of lung tissue. The overlay image shows the localization of the particles in close proximity to the nucleus of the cell. Figure 8 demonstrates the uptake of PS particles into alveolar macrophages as well as alveolar epithelial type II cells, which can be recognized by the occurrence of lipid bodies within the cells.

This project has received funding from the European Union's Horizon 2020 research and innovation programme under grant agreement No. 965196

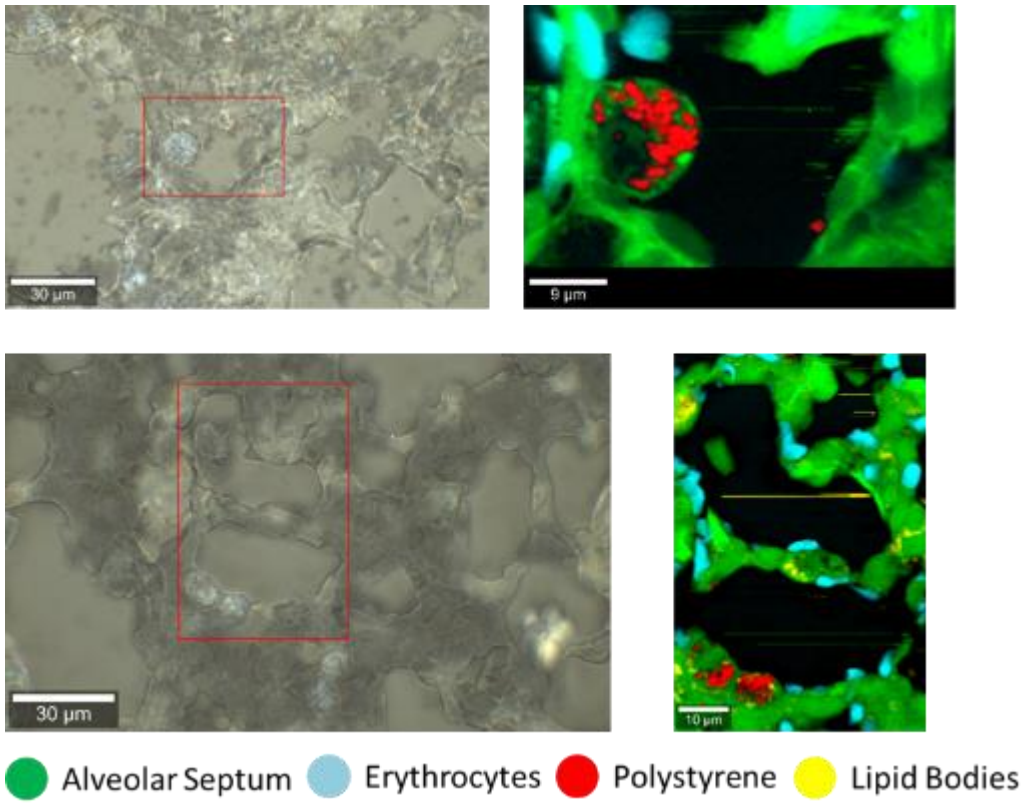

Figure 5: Analysis of lung tissue of mice exposed to PS particles for 24 hours. Bright-field image with the red highlighted areas subsequently measured by CRM (**left**). CRM mapping of PS uptake in alveolar macrophages in tissue section of a mouse exposed to 150 µg PS (**top right**) as well as in alveolar epithelial type II cells in the septum of tissue section of a mouse exposed to 50µg PS (**bottom right**).

3.2. 3D image of whole organism vs tissue slices

3D imaging of samples and the localization of particles is also feasible by CRM by the overlapping of several 2D images. Samples of drosophila larvae were investigated by CRM. The larvae were mounted on glass slides with nail varnish to prevent sample movement. For the dry measurement with the 532 nm laser a depth line scan was performed, where a spectrum was obtained every 5 µm. The recorded spectra did not contain tissue or PS related information due to sample burning and strong fluorescence (Figure 9). The measurement of whole drosophila immersed in PBS also yields no notable spectral information. One may assume that the high roughness of the sample makes it difficult to perform imaging in the lateral plane going through the tissue too deep, which caused the strong absorption of photons, or through the air spaces between the tissue protrusions. For the following studies, the larvae will be embedded in paraffin and slices at thickness of 5 to 10 µm will be analyzed as described above. This has been already proven in former studies for the analysis of metal particle uptake in gills, liver and intestine in adult zebrafish [7].

This project has received funding from the European Union's Horizon 2020 research and innovation programme under grant agreement No. 965196

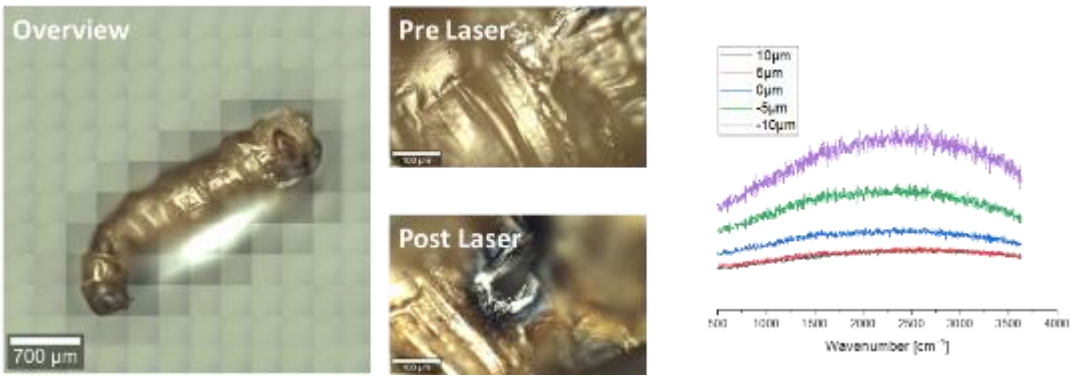

Figure 6: Dry measurement of whole drosophila larvae by 532 nm laser. Bright-field images of the whole larvae (**left**), enlarged ones before (**top middle**) and after measurement (**bottom middle**), and the recorded fluorescent signal in Raman spectra recorded by depth scans (**right**).

3.3. Broncho-alveolar lavage fluid from exposed mice

For the analysis of samples of BAL fluid from mice exposed to 150 µg of PS particles, a fraction of the BAL fluid was prepared on glass substrate using cytospin centrifugation. CRM measurements were performed under wet conditions. Figure 10 shows the uptake and the distribution of PS particles in individual cells of a small area of the BAL sample highlighted by the red line. These are likely to be macrophages, since the CH_2 intensity distribution shows a densely packed cytoplasm in these cells. The visualization allows the determination of particle uptake for single cells. Another approach utilizes a particle/cell counting software (WITec ParticleScout) for fast analysis of a large area of sample by recording one spectrum per cell (Figure 8). Figure 11 shows the selected Raman spectra recorded from red labelled cells in bright field image of the BAL sample. Intensities of the breathing mode of PS in the Raman spectra reflect different uptake rate of PS particles over population of selected BAL cells.

Since a large amount of data may be acquired with this method, the subsequent analysis by means of principal component analysis (PCA) is needed. The single spectra of 100 cells from control and exposed groups were compared and separated according to their spectral patterns by means of PCA. The results are shown in score plots, in which two principal components (PCs) are plotted against each other (Figure 12). Each point in this plot represents the spectrum of a single cell within an analyzed population. The loading plot shows which combination of vibrational modes mainly contributes to the separation of the cells into groups along the PCs. The analysis of the spectral marker for PS at 1001 cm^{-1} enables discrimination between cells with and without PS particles (Figure 9 top). The BAL cells from exposed and unexposed groups were separated in the score plot along PC-2. The score plot shows a clear discrimination between exposed and unexposed cells (red vs black points). The

This project has received funding from the European Union's Horizon 2020 research and innovation programme under grant agreement No. 965196

more right the cells are located in the score plot, the more particles are found in those cells. However, cells without PS particles can be also identified in the exposed cell population (red points in region of negative PC-2 in the score plot). Furthermore, PCA analysis was performed only for exposed group in order to get information about uptake rate across population of BAL cells from exposed mice (Figure 102 bottom). About 5 % of the analyzed cells have been found to have a high load of PS particles, while 20% showed a middle uptake rate. The rest of the cells, app. 75%, have taken up only few or no particles.

Additionally, exposed and control cells were compared by PCA using a spectral region above 1100 cm^{-1} without including PS breathing mode (Figure 10). Figure 13 shows the clear cell separation of two groups based on the lipid, protein and nucleus related bands, which indicates biochemical differences between the populations. The number of chosen cells and the number of mice used for these experiments is too low, to draw clear conclusions from it. However, this way of analyzing BAL cells can be promising in order to detect possible adverse effects after exposure to MNPLs.

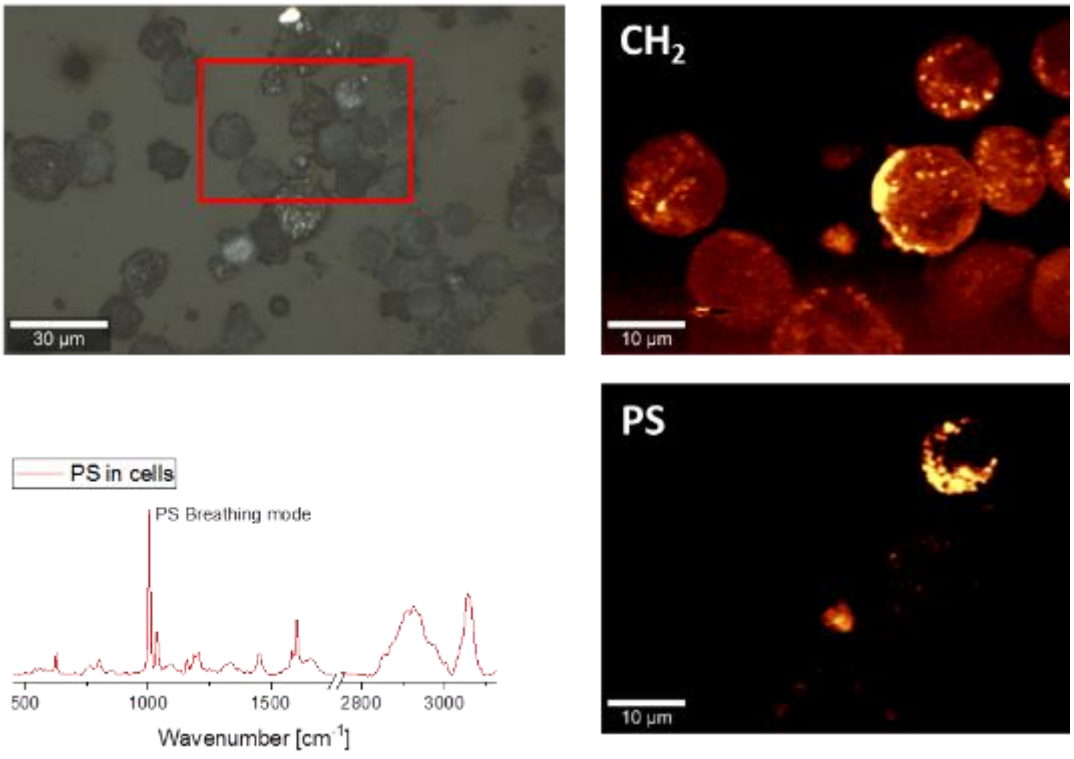

Figure 7: Analysis of BAL cells from mouse exposed to 150 µg PS particles for 24 hours. Bright-filed image of BAL sample (**top left**). CRM images visualize distribution of CH_2 intensity and PS particles within BAL cells over the measured area (red square) (**right**). Spectrum of internalized PS in the BAL cell (**bottom left**).

This project has received funding from the European Union's Horizon 2020 research and innovation programme under grant agreement No. 965196

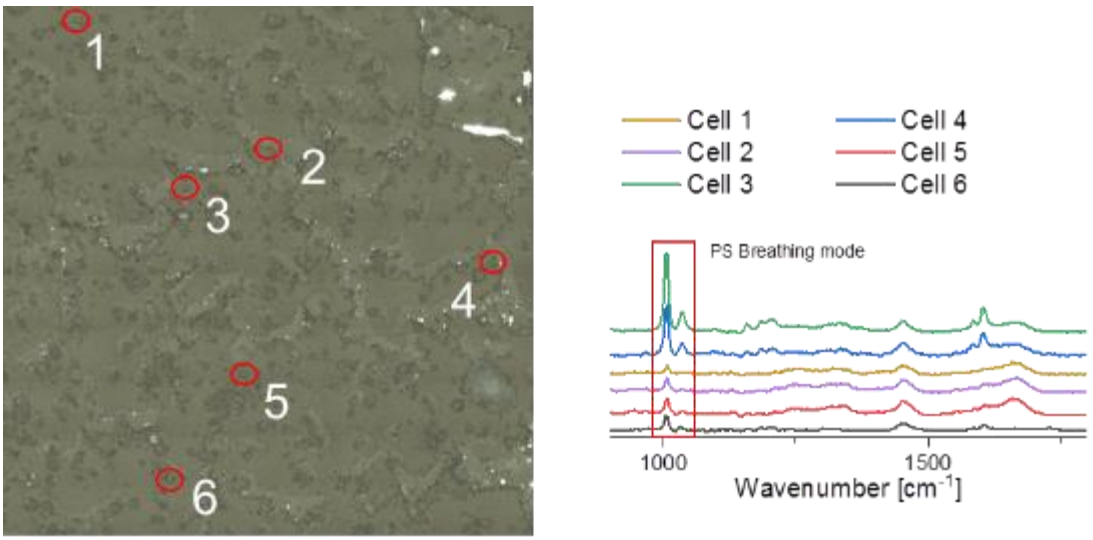

Figure 8: Detection of PS particles in BAL cells. Bright-filed image of BAL sample (**left**). Single Raman spectra of selected cells (red circles) are sorted by intensity of PS related vibration mode at 1001 cm^{-1} and demonstrate level of uptake in single cells (**right**).

This project has received funding from the European Union's Horizon 2020 research and innovation programme under grant agreement No. 965196

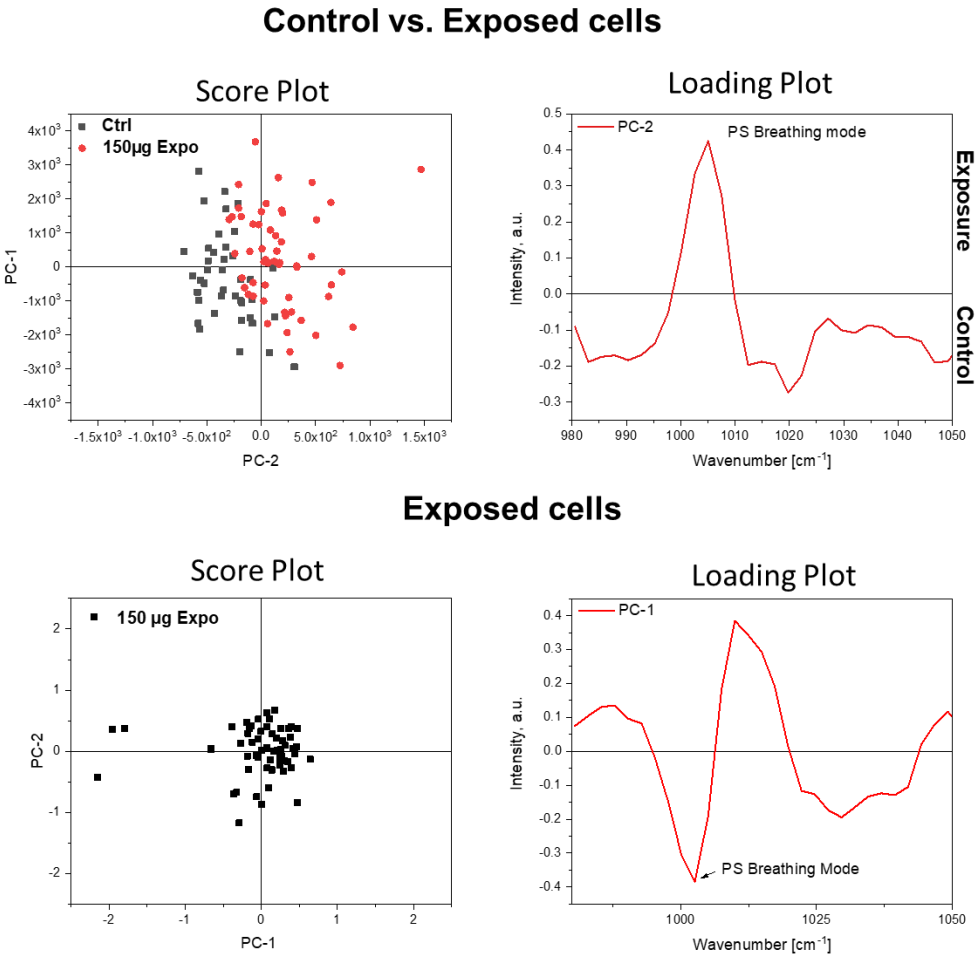

Figure 9: Principal component analysis of BAL cells from control and exposed groups of mice (150µg PS particles) in spectral region of 960 cm^{-1}- 1050 cm^{-1}. PCA score and loading plots from Raman spectra recorded from BAL cells of control vs exposed groups (top) as well from that of exposed group alone (bottom). The cell populations are separated along PC-1 and PC-2 components in score plots. These separations are displayed in loading plots.

This project has received funding from the European Union's Horizon 2020 research and innovation programme under grant agreement No. 965196

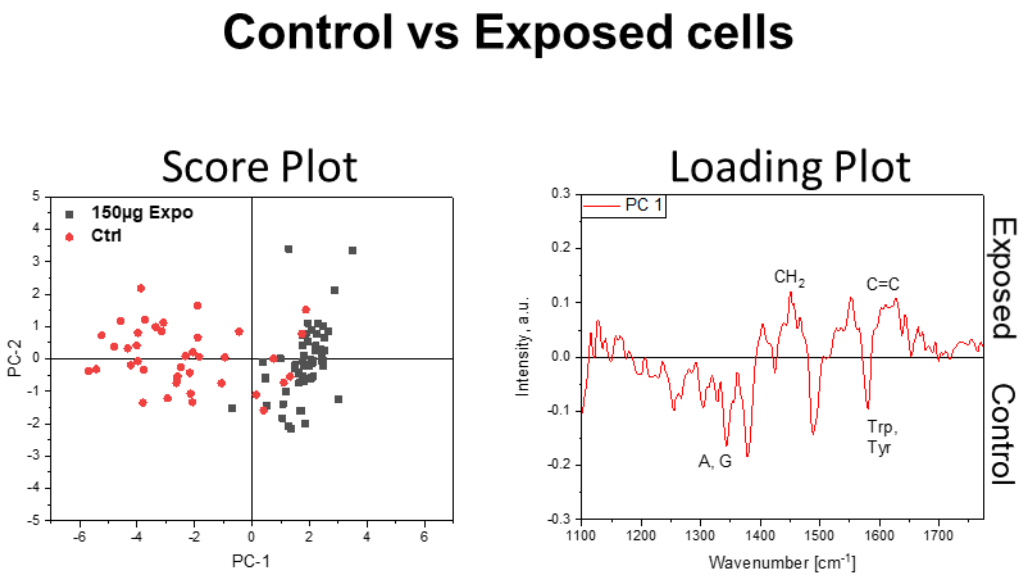

Figure 10: Principal component analysis of BAL cells from control and exposed groups of mice (150µg PS particles) in spectral region of 1100 cm^{-1}- 1780 cm^{-1}. When exposed and control cells are separated along PC-1 the score plot (left) based on their specific spectral pattern (right). Cells located on the right side in the scope plot (PC-1>0) are marked by increased expression of Raman bands that have a positive value in the loading plot (Intensity > 0); Cell located on the left side show an increased expression of Raman bands that have a negative value in the loading plot (Intensity <0).

4. Setup table

Table 1 shows the adapted parameters for detection of PS particles in biological matrices by applying 532 nm and 785 nm lasers. Both showed the capacity to detect PS particles in lung tissue sections. Although each of the tested lasers has advantages and disadvantages, the 532 nm produced the best results for lung tissue sections as well as BAL samples. The parameters must be chosen depending on the objective of measurements (Table 2). A fast screening approach aimed to detect particles in biomatrices requires short integration times and a large laser pinhole (100 µm) to obtain the maximum spectral information in a short amount of time. As this impairs the spatial resolution, the pinhole size must be reduced to 50 or 25 µm and the integration time has to be increased in order to achieve high-resolution imaging. A detailed spectral analysis would require an increased spectral resolution to avoid artefacts. For this, the detector grating has to be increased to 1800 g/mm. However, this reduces the intensity of the yielded spectra strongly.

This project has received funding from the European Union's Horizon 2020 research and innovation programme under grant agreement No. 965196

plasticheal

Table 1: Optimized and adapted set up parameters of CRM for detection and visualization of PS plastic particles in lung tissue of mice. The measurements were performed by using multi-mode fiber of 50 µm diameters and a grating of 600g/mm.

	532nm		785nm	
	dry	wet	dry	wet
Burning of organic matter	yes	no	no	
Fluorescence	yes		no	
Photoluminescence	no		yes	
Objective	50/0.8	63/1.0	50/0.8	63/1.0
Optimized Power	5 mW	37 mw	95 mW	
Integration time	0.3 s	0.07 s	0.3 s	
Substrate	glass, quartz, $CaFl_2$		quartz, $CaFl_2$	
Visualization of biomatrices	yes		yes	
PS visualization in biomatrices	yes		yes	

Table 2: CRM setup parameters for different scientific approaches at application of 532 nm laser. Fast screening allows the rapid detection of particles, with low spatial resolution. High resolution imaging enables the detailed mapping of biomolecules and particles. The detailed spectral analysis makes it possible to analyze possible adverse effects induced by particles.

	Fast Screening		High Resolution Imaging		Spectral Analysis	
	dry	wet	dry	wet	dry	wet
Laser power	5mW	37mW	5mW	37mW	5mW	37mW
Integration time	0.1s	0.03s	0.3s	0.07s	0.3s	0.1s
Grating	600g/mm		600g/mm		1800g/mm	
Pinhole	100µm		25µm, 50µm		25µm; 50µm	

This project has received funding from the European Union's Horizon 2020 research and innovation programme under grant agreement No. 965196

plasticheal

5. References

[1] C. Blucher, C. Zilberfain, T. Venus, N. Spindler, A. Dietrich, R. Burkhardt, S.C. Stadler, I. Estrela-Lopis, Single cell study of adipose tissue mediated lipid droplet formation and biochemical alterations in breast cancer cells, Analyst, 144 (2019) 5558-5570.
[2] X.L. Yan, T. Itoh, Y. Kitahama, T. Suzuki, H. Sato, T. Miyake, Y. Ozaki, A Raman Spectroscopy Study on Single-Wall Carbon Nanotube/Polystyrene Nanocomposites: Mechanical Compression Transferred from the Polymer to Single-Wall Carbon Nanotubes, J Phys Chem C, 116 (2012) 17897-17903.
[3] M. Mazilu, A.C. De Luca, A. Riches, C.S. Herrington, K. Dholakia, Optimal algorithm for fluorescence suppression of modulated Raman spectroscopy, Opt Express, 18 (2010) 11382-11395.
[4] M.A. Fikiet, D. Tuschel, V.V. Ermolenkov, I.K. Lednev, Clarifying Glass Luminescence at Near-Infrared Excitation, Appl Spectrosc, 74 (2020) 187-192.
[5] K. Hashimoto, V.R. Badarla, A. Kawai, T. Ideguchi, Complementary vibrational spectroscopy, Nature Communications, 10 (2019).
[6] K. Czamara, K. Majzner, M.Z. Pacia, K. Kochan, A. Kaczor, M. Baranska, Raman spectroscopy of lipids: a review, J Raman Spectrosc, 46 (2015) 4-20.
[7] M.L.F. Paolin Rocio Cáceres-Vélez, Elena Rojas, Thomas Meyer, Tom Venus, Cesar Koppe Grisolia, Irina Estrela-Lopis, Sergio Moya, Paulo César Morais, Ricardo Bentes Azevedo,, Impact of humic acid on the persistence, biological fate and toxicity of silver nanoparticles: A study in adult zebrafish, Environmental Nanotechnology, Monitoring & Management, Volume 12 (2019).

This project has received funding from the European Union's Horizon 2020 research and innovation programme under grant agreement No. 965196

plasticheal

ACRONYMS AND ABBREVIATIONS

CRM	Confocal Raman microscopy
PS	Polystyrene
MNPLs	Micro&nanoplastics
PBS	Phosphate buffered saline
PFA	Paraformaldehyde
BAL	Broncho-alveolar lavage
PC	Principal component
PCA	Principal component analysis

This project has received funding from the European Union's Horizon 2020 research and innovation programme under grant agreement No. 965196